Inhibition of CorA dependent Magnesium Homeostasis is cidal in Mycobacterium tuberculosis

Park, Yumi; Ahn, Yong-Mo; Jonnala, Surendranadha; Oh, Sangmi; Fisher, Julia M.; Goodwin, Michael B.

Published in:
Antimicrobial Agents and Chemotherapy

DOI:
10.1128/AAC.01006-19

Publication date:
2019

Document Version
Peer reviewed version

Inhibition of CorA dependent Magnesium Homeostasis is cidal in *Mycobacterium tuberculosis*.

Yumi Park[a*], Yong-Mo Ahn[a*], Surendranadha Jonnala[a], Sangmi Oh[a], Julia M. Fisher[a], Michael B. Goodwin[a], Thomas R. Ioerger[b], Laura E. Via[a], Tracy Bayliss[c], Simon R. Green[c], Peter C. Ray[c], Paul G. Wyatt[c], Clifton E. Barry 3[rd a], Helena I. Boshoff[a#]

[a]Tuberculosis Research Section, Laboratory of Clinical Immunology and Microbiology, National Institute of Allergy and Infectious Disease, National Institutes of Health, Bethesda, Maryland, USA

[b]Department of Computer Science and Engineering, Texas A&M University, College Station, Texas, USA

[c]Drug Discovery Unit, Division of Biological Chemistry and Drug Discovery, School of Life Sciences, University of Dundee, UK

Running Head: Magnesium Homeostasis by *M. tuberculosis* CorA

Address correspondence to Dr. Helena Boshoff, e-mail: hboshoff@niaid.nih.gov

*Present addresses: Yumi Park, Center for Personalized Precision Medicine of TB, Inje University College of Medicine, Busan, Republic of Korea; Yong-Mo Ahn, Department of Pharmacology, Physiology & Neuroscience, New Jersey Medical School, Rutgers, The State University of New Jersey, Newark, New Jersey, USA

YP and YMA contributed equally to this work

ABSTRACT

Mechanisms of magnesium homeostasis in *Mycobacterium tuberculosis* are poorly understood. Herein we describe the characterization of a pyrimidinetrione amide scaffold that disrupts magnesium homeostasis in the pathogen by direct binding to the CorA Mg^{2+}/Co^{2+} transporter. Mutations in domains of CorA that are predicted to regulate the pore opening in response to Mg^{2+} ions conferred resistance to this scaffold. The pyrimidinetrione amides were cidal against the pathogen under both actively replicating as well as non-replicating conditions *in vitro* and were efficacious against the organism during macrophage infection. However, the compound lacked efficacy in infected mice possibly due to limited exposure. Our results indicate that inhibition of Mg^{2+} homeostasis by CorA is an attractive target for tuberculosis drug discovery and encourage identification of improved CorA inhibitors.

INTRODUCTION

Short-course chemotherapy for tuberculosis was adopted by the WHO in 1991 for drug-sensitive disease; requiring 6 months of multi-drug treatment(1). The risk of drug-related toxicity as well as non-compliance increases proportionally over time which has motivated efforts to reduce the treatment duration(2). The current front-line drug regimen consists of drugs that target RNA synthesis (rifampicin), cell wall biosynthesis (isoniazid/ ethambutol) and pyrazinamide (which has an ill-defined mechanism of action) (3, 4). Identification of drugs that target novel pathways in the pathogen has been proposed as a way of developing new drug combinations that could reduce treatment duration(5). To this end, mechanisms that are critical for survival under various growth conditions are predicted to encompass targets that could lead to a rapid decline in bacterial viability *in vivo*.

Magnesium is an essential co-factor in a plethora of enzymatic reactions. It serves a structural role in the integrity of nucleic acids and proteins as well as maintaining the integrity of the cell membrane and cell wall(6, 7). In *M. tuberculosis* (*Mtb*) three mutants have been described that exhibited attenuation at low extracellular magnesium concentrations: *perM* encoding a membrane protein of unknown function, deletion of which results in *in vivo* attenuation and inability to grow at low Mg^{2+} concentrations; *phoP* encoding the transcriptional regulator of a two-component system important for complex lipid biosynthesis and virulence; and *mgtC* which encodes a P-type ATPase likely acting as an accessory protein for Mg^{2+} importdeletion of which results in an inability to grow at low Mg^{2+} concentrations at acidic pH and loss of virulence(8-10). The *in vivo* attenuation of these mutants in *Mtb*, as well as other

bacterial pathogens with inactivated Mg^{2+}-dependent processes, has been hypothesized to point to restriction of this essential cation, as a possibly host-mediated mechanism to control bacterial pathogens(7-10). Indeed, phagosomal Mg^{2+} concentrations at least during *Salmonella typhimurium* infection have been estimated to be in the 10-50 micromolar range(11). The predicted low phagosomal Mg^{2+} concentrations and the increased Mg^{2+} requirement of *Mtb* at low pH, suggests that access to this nutrient could be growth-limiting *in vivo.* Consequentially inhibitors of Mg^{2+} homeostasis would affect bacterial survival at every stage of host pathogenesis(12). The mechanisms by which *Mtb* maintains Mg^{2+} homeostasis are poorly understood. *Mtb* encodes two Mg^{2+} transporters, CorA and MgtE, neither of which is apparently essential based on saturating genome transposon mutagenesis studies(13, 14).

In this work, we describe the identification of a compound series that exerts potent growth inhibition of *Mtb* and inhibits Mg^{2+} uptake via direct binding to the CorA transporter. A representative of this inhibitor series lacked *in vivo* efficacy against *Mtb* in mice. This was presumed to be related to insufficient compound exposure *in vivo*.

RESULTS

Identification of a pyrimidinetrione amide with Gram-positive antibacterial activity

This series, as represented by Compound **1** was identified from a large whole cell phenotypic screen against *Mtb* and found to have potent antimycobacterial activity on two distinct growth media (Table 1). The pyrimidinetrione amide core is based on

88 barbituric acid. In order to establish some preliminary structure activity relationship
89 (SAR) analogues were prepared with different amines including a simple aniline (**2**),
90 cyclohexylamine (**3**), butylamine (**4**), benzylamine (**5**), 3-picolylamine (**6**). Except for
91 compound **2**, none showed equivalent antimicrobial activities in both media (Table 1).
92 Although compound **5** showed good potency in GAST medium (a minimal medium
93 lacking BSA), the lack of potency in 7H9 medium suggested high protein binding
94 discouraging further evaluation. The modification of the amide linker to generate either a
95 sulfonylamine (**7**) or a ketone (**8**) also resulted in complete loss of antitubercular activity.

96 Based on the initial SAR described in Table 1, a series of compounds modified in
97 the aniline moiety were further evaluated (Table 2). Interestingly, irrespective of the
98 substituents in the *para*-position of the aniline, compounds **9**–**14** showed good
99 antitubercular activities. Compounds **15** & **16** which had a substituent in the *ortho*-
100 position also showed activity. While other analogues with heteroaromatic rings instead
101 of a phenyl groups, such as pyridine (**17–19**) and isoxazole (**20**), generally had reduced
102 potency. Because the core is related to barbituric acid, we wanted to rule out non-
103 specific effects due to mitochondrial membrane depolarization(17). We tested for
104 cytotoxicity against HepG2 cells during growth on either glucose or galactose as sole
105 carbon source. Growth on galactose forces cells to use mitochondrial respiration to
106 generate ATP rather than through glycolysis as occurs during growth on glucose(18).
107 This showed that several of the compounds were associated with clear mitochondrial
108 toxicity; evidenced by the enhanced cytotoxicity of compounds during growth on
109 galactose. Cytotoxicity in galactose medium generally tracked with anti-mycobacterial
110 potency (Fig. S1). However, compounds having electron donating alkyl groups, methyl

(**9**) and isopropyl (**10**), were both selective and had no mitochondrial toxicity based on a lack of inhibition of HepG2 cell growth on either glucose or galactose.,

The compound series was not selectively anti-tubercular as seen by its broader-spectrum activity against *Mycobacterium smegmatis*, *Bacillus subtilis* and *Staphylococcus aureus* (Table S1). However, the series lacked activity against Gram-negative bacteria such as *Escherichia coli* and *Pseudomonas aeruginosa* (data not shown), suggesting a mechanism of action unique to Gram positive bacteria.

The pyrimidinetrione amide inhibits magnesium uptake in Mtb

In an effort to understand the mechanism of action of the series, resistant mutants were raised to compound **1**. Mutants were obtained at a frequency of resistance of 10^{-8}. Three that were confirmed to be more than 100-fold resistant to the compound, were submitted for whole genome sequencing. Two had independent mutations in *corA* (*Rv1239c*), *corA*:E212D and *corA*:A317S, other single nucleotide polymorphisms present showed no evidence of mechanism of action associated resistance (Table 3). The third mutant had an identical SNP profile to the second mutant suggesting that this mutant may have arisen as a sibling.

The *corA* gene encodes a putative magnesium and cobalt transporter predicted to be non-essential by genome-wide transposon mutagenesis studies(13, 14). To confirm that SNPs in *corA* were associated with resistance, we raised resistant strains to compounds (**1**, **10**, **12**, **13** & **15**) and specifically sequenced their *corA* gene. All resistant strains contained point mutations within the corA gene (Table S2). To interpret

133 the effect of these mutations on corA function, a MtCorA homology model was
134 generated from the crystal structure of *Thermotoga maritana* CorA (TmCorA) using
135 Phyre2(20). Unexpectedly the mutations did not occur at the divalent cation sensor
136 region where Mg^{2+} ions bind. Instead, the homology model predicted that the mutations
137 occurred within the acidic (E212D) and kink (G299S & M300V/L) regions which are
138 involved in the gating motion of CorA; and the hydrophobic tunnel (A317S) where Mg^{2+}
139 ions flow through (Fig. S2). The mutation data suggested that the pyrimidinetrione
140 amide scaffold affected the gating mechanism of CorA resulting in the inhibition of Mg^{2+}
141 uptake (Fig. S2). This hypothesis was supported by the Mg^{2+} dependence of the growth
142 inhibition in *Mtb* (Fig. 1A) as well as other Gram-positive bacteria (Table S2)

143 Co^{2+} was unable to rescue cells from pyrimidinetrione-dependent growth
144 inhibition (Fig. 1B). The inability of Co^{2+} to rescue growth inhibition was not surprising
145 since there are no known essential cobalt-dependent enzymes in *Mtb*. Magnesium is an
146 essential metal cofactor in many key metabolic enzymes and the specificity of some of
147 the pyrimidinetrione amides for inhibiting bacterial growth and not HepG2 cell growth
148 suggested that magnesium uptake could be a novel target for drug development.

149 To confirm that the series inhibited Mg^{2+} uptake, intracellular concentrations of
150 this cation were measured by inductively-coupled plasma mass spectrometry (ICP-MS).
151 This analysis confirmed that compound **10** treatment generated a concentration-
152 dependent decrease in intracellular magnesium levels (Fig. 1C). Moxifloxacin was
153 chosen as a negative control because it was not expected to affect cell wall or
154 membrane integrity both of which could potentially influence intracellular Mg^{2+} levels.

However, moxifloxacin resulted in an unexpected increase in intracellular magnesium concentrations (Fig. 1C) for reasons which were not clear.

The pyrimidinetrione amide- Mg^{2+} complex binds to the CorA transporter

The core of this series shows structural similarity to the pyrimidinedione scaffold associated with Mg^{2+} binding in drugs such as Raltegravir(21). To explore whether this series bound Mg^{2+} ions, we analyzed the UV-Vis spectral response of compound **10** upon titration with Mg^{2+} ions. A clear cation dependent decrease in absorbance at 280 nm was seen (Fig. S3). The coordination complex of compound **10** with Mg^{2+} was further investigated by NMR studies; based on the splitting pattern of the signals of the asymmetric pyrimidinetrione moiety, compound **10** forms the enol tautomer when interacting with Mg^{2+} (Fig. S4). The coordination of Mg^{2+} by this scaffold could suggest that the compounds merely act to deplete free Mg^{2+} ions with the *corA* mutations conferring higher affinity for the Mg^{2+}:$6H_2O$ complex. However, arguing against this notion, in the absence of compound the *corA* mutants required a 250-fold higher Mg^{2+} concentration to grow compared to the wild-type strain (Table S3).

In order to test whether the Mg^{2+}:pyrimidinetrione amide complex directly bound to CorA, we determined the thermal stability of recombinantly expressed CorA in the presence of Mg^{2+} and compound **10** (Fig. 2). This showed that all of these ligands increased thermal stability of the protein, indicating binding to the transporter (Fig. 2, Table 4). The apparent dissociation constant of CorA with metal ions and compound **10** was determined using fluorescence change based on tryptophan quenching (Fig. S5 and Table 5). The results indicated that Co^{2+} was poorly bound to CorA compared to Mg^{2+} whereas compound **10** bound with a 2-fold higher affinity than Mg^{2+} alone,

178 irrespective of the presence of Mg^{2+}. Although this result showed that
179 Mg^{2+}:pyrimidinetrione amide complex bound and stabilized the CorA structure, it was
180 still unclear how this event affected intracellular Mg^{2+} homeostasis, resulting in
181 bactericidality. We predicted that mutant strains such as *corA*:E212D could survive
182 exposure to compound **10** as a result of lower binding affinity of the CorA:E212D protein
183 to the Mg^{2+}:compound **10** complex, hereby overcoming the disruption of Mg^{2+}
184 homeostasis. Therefore, we performed similar thermal stability assays and fluorescence
185 shift assays using one of the mutant CorA proteins, the purified recombinant
186 CorA:E212, in the presence of Mg^{2+}, compound **10** or compound **10** with Mg^{2+}. The
187 assay result showed that the Mg^{2+}:pyrimidinetrione amide complex could also bind to
188 the mutated CorA:E212D (Table S4 and S5). This result suggested that the observed
189 mutations on CorA do not have a measurable effect on the binding affinity of the
190 Mg^{2+}:pyrimidinetrione amide complex to this transporter (bearing in mind the limited
191 analytical sensitivity of these assays).

192 *The pyrimidinetrione amide decreases Mtb viability in vitro and ex vivo but lacks*
193 *apparent in vivo efficacy*

194 The pyrimidinetrione amide compound **10** was cidal against actively growing *Mtb* cells
195 showing a 2-log kill over a week of exposure even at concentrations as low as 2-fold the
196 MIC value. Higher concentrations resulted in a more rapid cidal effect with no detectable
197 viable cells remaining as determined by colony counts on solid agar (Fig. 3A). We next
198 sought to interrogate the importance of Mg^{2+} uptake under non-replicating conditions
199 using a non-replicating persistence induced by adaptation to hypoxia with subsequent
200 exposure of cells to compounds under anaerobic conditions. This showed that Mg^{2+}

uptake was critical under these conditions as evidenced by the greater than 3-log kill after a week of compound exposure (Fig. 3B).

The cidal consequence of disrupting Mg^{2+} homeostasis during active growth as well as non-replicating persistence prompted us to explore their anti-tubercular effect during parasitism of host macrophages. We selected compounds that had no general cytotoxic or mitochondrial toxic effect (compounds **9** and **10**), no general cytotoxic yet with a limited mitochondrial toxicity giving a 10-fold selectivity window (compound **16**) or with limited general cytotoxicity and higher mitochondrial toxicity that still gave us a higher than 10-fold selectivity window (compound **1**) (Table 1). All of these compounds exerted time- and dose-dependent intracellular (*ex vivo*) killing of *Mtb* growing in macrophages (Fig. 3C).

The promising activity of compound **10** against *Mtb* during growth in macrophages encouraged us to explore its *in vivo* efficacy. Preliminary phamacokinetic (PK) analysis indicated the half-life of compound **10** was 2.5 h ± 0.4 when dosed once daily indicating that at least twice per day (BID) dosing was needed. Unfortunately, this compound was intolerable to mice at high (100 mg/kg) doses. At 30 mg/kg, dosed BID by oral gavage, the compound achieved an AUC of 56 μg*h/mL which gave a AUC/MIC ratio of 250 and plasma concentrations that were almost 10-fold above MIC concentrations at the first trough and just above MIC at 24h (0.3 μg/mL ± 0.16 SD; Fig. 4A). This dosing schedule was tolerable in naïve mice. Subsequently, *Mtb*-infected mice were treated with 30 or 15 mg/kg BID, however, after multiple BID doses, 30 mg/kg was intolerable to the infected mice necessitating a deescalation to 30 mg/kg once per day for that group for the remaining dosing period. Due to adverse effects, compound **10**

could not be administered at higher concentrations and at the highest tolerable concentration, it lacked efficacy after 2 and 4 weeks of treatment in infected mice lungs (Fig. 4B) and spleens (results not shown).

DISCUSSION

We have identified a pyrimidinetrione amide scaffold with potent *in vitro* activity against *Mtb*. Resistant mutants mapped to the CorA transporter with Mg^{2+} supplementation abrogating the growth inhibition in a concentration-dependent fashion. Using thermostability assays and fluorescence shift assays, we were able to demonstrate that this inhibitor binds to CorA in the presence and absence of Mg^{2+}. The ligand binding site for this inhibitor remains to be identified but we were also able to show that resistance-conferring amino acid mutations had no effect on this ligand binding. Instead, the mutations mapped to the acidic and kink regions of the cytoplasmic domain of the CorA transporter which are involved in the gating motion of the pore, indicating that mode of resistance were not due to changes in CorA-ligand interaction, but likely as a result of perturbation of the gating motion in response to Mg^{2+} dissociation from the protein. Low cytosolic Mg^{2+} concentrations result in cation dissociation with resultant channel opening driven by this gating mechanism. In line with a loss of regulation of the pore opening of the cation channel, the *corA*:E212D and *corA*:A317 mutants required a 250-fold higher Mg^{2+} concentration in the medium than parental wild-type cells for growth (results not shown). During preparation of this manuscript, a report was published that found similar mutations in CorA to a pyrimidinetrione as well as 4-hydroxyquinoline scaffold(19). These mutations were predicted to result in channel opening thereby resulting in increased cytosolic Mg^{2+} concentrations. Similar to our work, cytosolic

247 concentrations of both free and bound Mg^{2+} were decreased complementing our data
248 that these inhibitors directly influence the influx/efflux of this cation.

249 The observation that the metabolic consequence of CorA inhibition is both growth arrest
250 and death was surprising since there is an alternative Mg^{2+} transporter encoded by
251 *mgtE* in the bacterium. The finding that only mutations in *corA* could confer resistance
252 suggests that regulation of Mg^{2+} homeostasis by this cation is predominantly conferred
253 by the CorA transporter where changes in MgtE levels do not occur rapidly enough to
254 overcome this dysregulation of Mg^{2+} homeostasis. In contrast, during genetic
255 inactivation of *corA,* compensatory genetic changes could occur to alter levels of MgtE
256 as cells are gradually depleted of CorA protein. The finding that *corA* but not *mgtC* or
257 mgtE is conserved in *Mycobacterium leprae*, a mycobacterium with a minimal genome,
258 points to the conserved nature of Mg^{2+} homeostasis by this transporter. Despite this,
259 there is no evidence for the *in vivo* essentiality of *Mtb corA* during mouse
260 pathogenesis(22). Intriguingly, these compounds were only active against Gram positive
261 bacteria tested and not Gram negatives. CorA is widely distributed in bacteria including
262 *E. coli* and *P. aeruginosa*(6). Lack of activity against these Gram negative microbes
263 could be due to lack of binding to their CorA counterpart, different mechanisms of Mg^{2+}
264 homeostasis, lack of transport of the pyrimidinetrione amides across the outer
265 membrane or their efflux by multidrug efflux pumps.

266 Our results emphasize the importance of Mg^{2+} homeostasis during active
267 replication as well as non-replicating persistence *in vitro* and also during parasitism of
268 host macrophages. Free Mg^{2+} concentrations in the lung were determined to be 0.67 ±
269 0.08 mM (data not shown), a value similar to reported concentrations in plasma(23),

which is below the level that overcomes the growth inhibition by the pyrimidinetrione amides. The lack of *in vivo* efficacy was disappointing although the pharmacokinetic studies suggested that blood serum concentrations were only sufficiently above the MIC for half of the dosing period when extrapolated from the PK parameters (Fig. 4A). The concentration of compound in the cellular lesions may further be well below the MIC level during this dosing period. In addition, despite the lack of cytotoxicity of the compound, clinical signs of toxicity were evident when mice were dosed at 100 mg/kg (results not shown) prohibiting additional studies to probe the *in vivo* efficacy of this compound.

In conclusion, our results demonstrate the critical role of CorA in maintaining Mg^{2+} homeostasis and its attractiveness as a drug target. Despite the *in vitro* and *ex vivo* efficacy of the pyrimidinetrione amides, our data suggests that an alternative scaffold that inhibits CorA function would need to be identified in order to perform the proof of concept experiments that establish the validity of this target *in vivo*.

MATERIALS AND METHODS

Chemistry. All chemicals and reagents were purchased from Aldrich (Sigma Aldrich, St. Louis, MO, USA), Lancaster (Alfa Aesar, Johnson Matthey Company, Ward Hill, MA, USA) and were used without further purification. Comercially available analogues of pyrimidinetrione amide were purchased from Enamine LLC (NJ, USA), Bionet America, Inc. (CA, USA), and MicroCombiChem GmbH (Wiesbaden, Germany). Reactions were monitored by TLC, performed on silica gel glass plates containing 60 GF-254, and

visualization on TLC was achieved by UV light or iodine indicator. Column chromatography was performed with Merck (60-120) mesh silica gel. ^{1}H NMR spectra were recorded on Varian Mercury-300 NMR Spectrometer and chemical shifts are reported in ppm downfield from internal TMS standard. Routine mass analyses (LRMS) were performed on HP Agilent LC/MS series 1100 system equipped with a reverse phase column (Agilent Poroshell 120 EC-C18, 2.7 µm, 50 × 2.1 mm) and photodiode array detector using electrospray ionization (ESI). All the reported compounds were pure and > 95%.

Synthesis of compound ***12****,* ***14****–****20***(24)

To a solution of 1,3-dimethylpyrimidine-2,4,6(1*H*,3*H*,5*H*)-trione (1.0 eq) in DCM (0.1 M) was added pyridine (1.2 eq) and 4-dimethylaminopyridine (0.1 eq) at 0°C. Ethylcarbonochloridate (1.0 eq) was added dropwise to the reaction mixture at the same temperature over 1h. After stirring for 12 h at 0°C, the reaction mixture was allowed to warm to room temperature and then diluted with DCM and washed with water. The organic layer was dried over Na_2SO_4 and evaporated *in vacuo*. The crude mixture was recrystallized from ethanol to get ethyl 1,3-dimethyl-2,4,6-trioxohexahydropyrimidine-5-carboxylate as a white solid (1.09 g, 75%). ^{1}H NMR (DMSO-d_6, 300 MHz) δ 4.28 (qt, J = 6.9 Hz, 2H), 3.16 (s, 3H), 1.27–1.23 (t, J = 6.9 Hz, 3H); LCMS (ESI) *m/z* 229 $[M+H]^+$.

To a solution of ethyl 1,3-dimethyl-2,4,6-trioxohexahydropyrimidine-5-carboxylate (1.0 eq) in toluene (0.5 M) was added each amine (1.0 eq) and TEA (1.2 eq). The reaction mixture was refluxed for about 12 h. After cooling down to room temperature, the reaction mixture was diluted with ethyl acetate and then washed with water. The organic

layer was dried over Na_2SO_4 and evaporated *in vacuo*. The crude mixture was recrystallized from acetonitrile to get the desired products, **12**, **14**–**20**.

1,3-Dimethyl-2,4,6-trioxo-N-(4-phenoxyphenyl)hexahydropyrimidine-5carboxamide (**12**). White solid (75%): ^{1}HNMR ($CDCl_3$, 300 MHz) δ 11.92 (s, 1H), 7.46 (d, *J* = 6.9 Hz, 2H), 7.35 (t, *J* = 7.2 Hz, 2H), 7.12 (t, *J* = 7.5 Hz, 1H), 7.03–7.00 (m, 4H), 3.41 (s, 3H), 3.38 (s, 3H); LCMS (ESI) *m/z* 368 $[M+H]^+$.

N-(4-acetylphenyl)-1,3-dimethyl-2,4,6trioxohexahydropyrimidine-5-carboxamide (**14**). White solid (79%): ^{1}HNMR ($CDCl_3$, 300 MHz) δ 12.10 (s, 1H), 7.97 (d, *J* = 8.7 Hz, 2H), 7.63 (d, *J* = 8.7 Hz, 2H), 3.41 (s, 3H), 3.37 (s, 3H), 2.59 (s, 3H); LCMS (ESI) *m/z* 318 $[M+H]^+$.

N-(4-bromo-2-fluorophenyl)-1,3-dimethyl-2,4,6-trioxohexahydropyrimidine-5-carboxamide (**15**). White solid (46%): ^{1}HNMR ($CDCl_3$, 300 MHz) δ 12.04 (s, 1H), 7.98 (t, J = 8.5 Hz, 1H), 7.38–7.26 (m, 2H), 3.42 (s, 3H), 3.38 (s, 3H); LC-MS: LCMS (ESI) *m/z* 370 $[M-H]^-$.

1,3-Dimethyl-2,4,6-trioxo-N-(2,4,6-trichlorophenyl)hexahydropyrimidine-5-carboxamide (**16**). White solid (48%): ^{1}HNMR ($CDCl_3$, 300 MHz) δ 11.35 (s, 1H), 7.44 (s, 2H), 3.40 (s, 3H), 3.39 (s, 3H); LCMS (ESI) *m/z* 378 $[M+H]^+$.

N-(6-chloropyridin-3-yl)-1,3-dimethyl-2,4,6trioxohexahydropyrimidine-5-carboxamide (**17**). White solid (88%): ^{1}HNMR ($CDCl_3$, 300 MHz) δ 11.94 (s, 1H), 8.52 (d, , *J* = 2.4 Hz, 1H) 8.01–7.96 (dd, *J* = 2.7 and 8.7 Hz , 1H), 7.35 (d, *J* = 8.4 Hz, 1H), 3.41 (s, 3H), 3.37 (s, 3H); LCMS (ESI) *m/z* 311 $[M+H]^+$.

335 *1,3-dimethyl-N-(6-methylpyridin-2-yl)-2,4,6-trioxohexahydropyrimidine-5-carboxamide*
336 (**18**). White solid (71%): ^{1}HNMR ($CDCl_3$, 300 MHz) δ 12.13 (s, 1H), 7.70 (d, *J* = 7 Hz,
337 1H), 7.63 (t, *J* = 7.8 Hz, 1H), 6.98 (d, *J* = 7.5 Hz, 1H), 3.39 (s, 6H), 2.50 (s, 3H); LCMS
338 (ESI) *m/z* 291 $[M+H]^+$.

339 *1,3-Dimethyl-2,4,6-trioxo-N-(4(trifluoromethyl)pyridin-2-yl)hexahydropyrimidine-5-*
340 *carboxamide)* (**19**). White solid (73%): ^{1}HNMR ($CDCl_3$, 300 MHz) δ 12.18 (s, 1H), 8.55
341 (d, *J* = 5.1 Hz, 1H), 8.27 (s, 1H), 7.32 (d, *J* = 4.8 Hz, 1H), 3.43 (s, 3H), 3.39 (s, 3H);
342 LCMS (ESI) *m/z* 345 $[M+H]^+$.

343 *1,3-Dimethyl-N-(5-methylisoxazol-3-yl)-2,4,6-trioxohexahydropyrimidine-5-carboxamide*
344 (**20**). White solid (69%): ^{1}HNMR ($CDCl_3$, 300 MHz) δ 12.04 (s, 1H), 6.52 (s, 1H), 3.41 (s,
345 3H), 3.36 (s, 3H), 2.43 (s,3H); ^{13}C NMR (CDCl3, 75 MHz) δ 169.1, 167.8, 162.8, 161.7,
346 158.4, 91.7, 81.6, 28.5, 12.1; LCMS (ESI) *m/z* 281 $[M+H]^+$.

347 *Strains, media, and materials. Mtb* H37Rv (ATCC 27294) was used for all experiments.
348 To determine the antimicrobial spectrum of the compounds, *B. subtilis* and *S. aureus*
349 was used as gram positive strains, *E. coli* and *P. aeruginosa* were used as gram
350 negative strains. For liquid cultures, *Mtb* was grown in 7H9 medium which consists of
351 Middlebrook 7H9 (Becton Dickinson) broth base supplemented with ADC [albumin
352 (50 g/L)/dextrose (20 g/L)/NaCl (8.1 g/L)], 0.2% glycerol] and 0.05% Tween 80. Solid
353 agar media (7H11/OADC) for *Mtb* growth consisted of Middlebrook 7H11 (Becton
354 Dickinson) agar base supplemented with OADC [ADC with 0.06% oleic acid]. GAST
355 (glycerol-alanine-salts-Tween 80) was used as defined minimal liquid growth media for
356 *Mtb(25)*. Mg^{2+}-free GAST media made by omitting $MgCl_2$:$6H_2O$ from the medium

composition. The low pH nitrosative stress medium contained bovine serum albumin fraction V (5 g/L)/butyric acid (2.5 mM)/$NaNO_2$ (6.9 mg/mL)/NaCl (0.81 g/L)/0.05% Tyloxapol, pH adjusted to 6.0. MIC determination was performed as previously described(25). Luria-Bertani (LB) broth (Difco, New Jersey, USA) was used for MIC of Gram positive and negative strains. The screening conditions under which the original pyrimidinetrione hits were identified have been previously described but in brief consisted of 7H9 medium with readout of *Mtb* growth after 3 days of compound exposure(26).

*Generation and characterization of pyrimidinetrione resistant mutants.*To generate spontaneously resistant mutants to the compounds, 50 ml of *Mtb* was grown to OD_{650nm} 0.2. Harvested cells were resuspended in 500 µL of media and 100 µL aliquots (10^9 cells) plated on 7H11/OADC containing compound **1** at concentrations corresponding to 5x, 10x, 20x MIC. Appropriate dilutions of the cell suspensions were also plated on drug-free plates to calculate bacterial numbers in the suspensions for determination of frequencies (resistance frequency being the number of resistant mutants obtained per number of bacteria plated). Agar plates were incubated at 37°C for 4 weeks. After 4 weeks, 4 colonies growing on 7H11/OADC containing 10x MIC compound **1** were inoculated in 7H9 media and resistance confirmed by MIC determination. Genomic DNA of mutants was isolated by the CTAB method(27). Whole genome sequencing was performed and analyzed as described(28).

Cytotoxicity in HepG2 cells. Cytotoxicity in HepG2 cells was measured by CellTiter-Glo™ Luminescent Cell Viability Assay (Promega). For glucose media, 20,000 HepG2 cells were seeded in 96 well white flat-bottom plates (Corning incorporated) in DMEM

GlutaMAX (Gibco) supplemented with 10% fetal bovine serum, 20 mM HEPES, and 0.5 mM sodium pyruvate. For galactose media, HepG2 cells were pre-cultured in galactose DMEM and seeded in same plate with glucose media. Galactose DMEM consists of glucose-free DMEM (Gibco) supplemented with 10% fetal bovine serum, 10 mM D-galactose, 2 mM L-glutamine, 5 mM HEPES, and 0.5 mM sodium pyruvate. The plates were incubated at 37°C with 5% CO_2. The following day, 2-fold serial dilutions of compound up to 100 µM were added in the respective growth medium in duplicate and cells incubated for 24 hours. After this, 20 µL of CellTiter-glo reagent was added to each well followed by incubation at 37°C with 5% CO_2 for 10 min. Cytotoxicity was determined by measuring luminescence using Fluostar Optima FL (BMG Labtech).

In Silico Analysis. Amino acid sequence of *Mt*CorA (Rv1239c) was retrieved from Mycobrowser database (https://mycobrowser.epfl.ch/). FASTA format of MtCorA protein sequence was submitted to PHYRE2 protein fold recognition server. Ninty nine sequence alignment hits were obtained. The sequence of TmCorA was selected as a single highest scoring template and 332 residues (91% of MtCorA sequence) were modelled with 100% confidence by the structure of TmCorA.

Magnesium and cobalt concentration dependent MIC. We used Mg^{2+}-free GAST media to test the magnesium-dependence of the MIC of the compounds. Two-fold concentrated GAST generated without the addition of magnesium chloride hexahydrate was prepared. An equal volume of magnesium chloride in sterile distilled water was added to the GAST medium to give final concentrations ranging from 0.12 mM up to 240 mM. MIC determinations for the compounds were set up in duplicate as previously described for each $MgCl_2$ concentration(29). Briefly, an equal volume of medium (50 µL

GAST at the defined $MgCl_2$ concentration) with compound serially diluted in duplicate from 50 to 0.024 µM was added to wells of a round-bottom 96-well plate (Nunclon). *Mtb* culture in GAST at OD_{650nm} of 0.2 was diluted 1: 500 in 2x Mg^{2+}-free GAST and 50 µL added to each well of the 96 well plates. Plates were incubated under 5% of CO_2 at 37°C. Growth was measured using an inverted enlarging mirror at 1, 2 and 3 weeks with MIC taken as the concentration that completely inhibited all visible growth. For cobalt dependent MIC test, $CoCl_2$ was added in GAST media from 0.001 to 5 mM concentration and MIC performed as above.

Magnesium concentration measurement by inductively coupled plasma - mass spectroscopy (ICP-MS). We measured magnesium concentrations in *Mtb* cells treated by inductively coupled plasma - mass spectroscopy (ICP-MS). Two liters of *Mtb* was grown to OD_{650nm} 0.6 in 7H9. Five hundred milliliter of culture volumes were incubated with 1x, 10x MIC of compound **10**, 10x MIC of moxifloxacin or an equivalent volume of DMSO vehicle control (0.1% v/v) for 24 hours in 2 L capacity rolling bottles. Cells were harvested and washed three times with 1/10 volume phosphate buffered saline containing 0.05% Tween 80 (PBST). The wet weight of *Mtb* cell pellets was recorded to normalize magnesium concentration prior to autoclaving. ICP-MS analysis was serviced by Elementary Analysis Inc. (Lexington, KY, USA)

UV spectrum scanning to test magnesium binding of pyrimidinetrione. One milliliter of 100 µM **10** dissolved in 100 mM HEPES buffer was filled in 1 cm path length quartz crystal cuvettes for UV scanning. The absorbance of the compound **10** solution was scanned from 200 nm to 400 nm wavelengths by a Varian Cary 300 Bio UV/VIS spectrophotometer. We sequentially added 10 µL of 1 mM MgSO4 to the compound

426 solution to observe changes in absorbance spectrum. A standard curve was plotted with
427 A_{280nm} of 5, 10, 50 and 100 µM of compound **10**. Absorbance at 280 nm was used to
428 calculate compound **10** after correcting for changes in volume and plotted in a graph.

429 *Minimum magnesium requirement test. Mtb* H37Rv, *corA*:E21D, and *corA*:A317S
430 strains were cultured in GAST to OD_{650nm} 0.2 at 37°C. Fifty microliter of Mg^{2+}-free
431 GAST was distributed in every well of a round-bottom 96-well plate (Nunclon). Fifty µL
432 of 240 mM of $MgCl_2$ dissolved in Mg^{2+}-free GAST was added to the wells of the first
433 column of this plate and 50 µL volumes transferred from column 1 to column 12
434 generating a 2-fold serial dilution series of $MgCl_2$ across the plate. *Mtb* cultures were
435 diluted 1: 500 in Mg^{2+}-free GAST and 50 µL added to each well of the 96 well plates.
436 Growth was measured using an inverted enlarging mirror at 1, 2 and 3 weeks with the
437 minimum Mg^{2+} concentration to support growth taken as the lowest concentration that
438 supported evidence of any visible growth.

439 *Cloning, expression and purification of MtCorA.* The *M. tuberculosis* corA gene,
440 *rv1239c,* was cloned into the pET28a vector. The gene was amplified by PCR using
441 Herculase II Fusion DNA polymerase (Agilent) and the following primers: forward-5'-
442 CGCGGCAGCCATATGTTCCCAGGGTTT-3' and reverse-5'-
443 TGCGGCCGCAAGCTTCTAGAGCCAGTTTCT-3'.The PCR-amplified gene was
444 inserted between two restriction sites, *Nde*I and *Hin*dIII, using In-Fusion® HD Cloning
445 Plus (Takara). Site-directed mutagenesis to obtain gene encoding *corA*:E212D mutant
446 was performed. MtCorA contained the N-terminal poly-histidine tag. The plasmids
447 carrying the wildtype and mutant *corA* gene were transformed into in OverExpress™
448 C41(DE3) (Lucigen). The cells were grown in LB media at 37ºC. The induction was

initiated with 1mM IPTG at OD_{600nm} 0.7-0.8 and after 6 h, the cells were harvested by centrifugation at 3500 rpm for 20 min. The cell pellet was resuspended in lysis buffer containing 50 mM Tris-HCl pH 8.0, 150 mM NaCl, 0.5 mM DTT and SIGMAFAST™ Protease Inhibitor Cocktail Tablets, EDTA-Free (Sigma-Aldrich). After sonication, the lysed cells were pelleted by centrifugation at 20,000 g for 60 min and the membrane was isolated from the supernatant by ultracentrifugation at 142,000 g for 60 min. The isolated membrane was then solubilized in the resuspension buffer, 50 mM Tris-HCl pH 8.0, 300 mM NaCl, 20 mM imidazole, 0.5 mM DTT, with 1% (w/v) dodecyl maltoside (DDM) (Anatrace). The resulting supernatant was loaded onto a Ni-NTA column. The column was washed with wash buffer consisting of 50 mM Tris-HCl pH 8.0, 300 mM NaCl, 40 mM imidazole, 0.5 mM DTT, with 0.1% (w/v) DDM. The CorA or CorA mutant protein was eluted with elution buffer (50 mM Tris-HCl pH 8.0, 300 mM NaCl, 300 mM imidazole, 0.5 mM DTT, with 0.05% (w/v) DDM) and the resulting supernatant fractions containing CorA were identified using SDS-PAGE, pooled and dialyzed against dialysis buffer (50 mM Tris-HCl pH 8.0, 100 mM NaCl, 0.5 mM DTT, with 0.05% (w/v) DDM).The protein was finally purified on a Superdex 200 16/60 (GE Healthcare) in 50 mM Tris-HCl pH 8.0, 300 mM NaCl, 0.5 mM DTT, with 0.05% (w/v) DDM.

Thermostability test of CorA with pyrimidinetriones. Purified MtCorA samples were diluted to a concentration of 0.5 mg/mL. The solution was aliquoted into 30 µl volumes, with 1 µL of a stock solution of different Mg^{2+} concentrations added to the aliquot. Samples were incubated for 20 min at room temperature and then further incubated for 10 min at every increment of 5°C up to 95°C in a thermocycler. The samples were

transferred to a 96-well filter plate (0.45 µm) (Millipore) to remove precipitated proteins. The yield of the filtered protein was analyzed by SDS/PAGE.

Substrate Binding Measured by Fluorescence Quenching. The dissociation constants between CorA and its ligands, Mg^{2+}, Co^{2+} and compound **10**, were determined by the ligand dose-dependent fluorescence quenching assay (Cary Varian Eclipse fluorescence spectrophotometer). CorA was titrated with increasing concentrations of ligands and fluorescence emission was measured at ~350 nm following excitation at 283 nm (bandwidths of 5nm). The fluorescence quenching ΔF versus ligands concentration [S] was plotted and K_d(app) of CorA to ligands were calculated by fitting the data to an equation,

$$\Delta F = (F_0 - F) = \frac{\Delta F_{max} * [S]}{K_d(app) + [S]}$$

where F_0 and F are the fluorescence intensities in the absence and presence of substrates, respectively, [S] is the ligand concentration, and K_d(app) is the apparent dissociation constant of CorA to ligands.

Efficacy study in vitro, ex vivo and in vivo. In vitro efficacy of compounds against *Mtb* was measured during aerobic growth as well as during anaerobic non-replicating persistence. Time kill kinetics were measured under aerobic conditions as follows. Logarithmically growing *Mtb* (OD_{650nm} 0.2) was diluted 1,000-fold in 7H9 media and 1 ml volumes exposed to 1x, 2x, 5x, 10x, and 20 x MIC compound **10** up to 7 days in duplicates. Samples were collected and plated on 7H11/OADC plates for CFU enumeration at 1, 2, 4 and 7 days of treatment. For anaerobic conditions, *Mtb* was cultured in the self-generated oxygen-depletion model as previously described(29).

One milliliter volumes of anaerobic *Mtb* culture was exposed 1 week to 1x, 5x, 10x, 20x and 50x MIC compounds **9**, **10**, and **20** in an anaerobic chamber (Microbiology International) followed by CFU enumeration as above.

For *ex vivo* efficacy testing, J774 cells (6.6 x 10^4 cells/well) were seeded in flat-bottom 24 well plates (Corning incorporated) in J774 growth medium consisting of DMEM GlutaMAX (Gibco) supplemented with 10% fetal bovine serum, 20 mM HEPES + 0.5 mM sodium pyruvate. *Mtb* H37Rv with confirmed high levels of phthioceral dimycocerosate was grown in 7H9 to an OD_{650nm} of 0.5, filtered through a 5 μm sterile filter to ensure a single cell suspension, cell density confirmed at OD_{650nm}, and diluted in J774 growth medium to 4.4 x 10^5 CFU/mL. Aliquots of 0.1 mL of the *Mtb* suspension was added to each well of the 24-well plate giving an MOI 1:1.5. After overnight incubation, medium was aspirated and monolayers were washed twice in pre-warmed PBS (pH 7.4) twice. At this point, four wells were used for CFU enumeration as described below. To the remaining wells, 1mL J774 growth medium containing compound or vehicle (DMSO) control was added to each well. Each compound was tested at 1, 5, and 10-fold its MIC concentration in duplicate wells for each time point and concentration. Rifampicin (0.5 and 5 μg/mL) was used as positive control. Cells were incubated at 37°C, 95% humidity, 5% CO_2 incubator for 3 and 7 days. Media was replenished at days 3 and 5 taking care not to remove any macrophages since the pyrimidinetrione amides resulted in loss of adherence of macrophages over time. After 3 or 7 days of incubation, medium was removed taking care notremove macrophages and 1mL of 7H9 medium containing 0.1% SDS added to each well to ensure macrophage lysis. After 5 minutes, lysate was rapidly mixed to shear eukaryotic DNA, diluted in 7H9

and plated on 7H11/OADC plates. Colony counts were enumerated after 4 weeks of incubation at 37°C.

Mouse studies were carried out in accordance with the Guide for the Care and Use of Laboratory Animals of the National Institutes of Health under Animal study protocol numbers LCIM 4E. Pharmacokinetic analyses on 20 C57BL/6J mice were done by administering 30 mg/kg compound **10** suspended in 10% (2-Hydroxypropyl)-β-cyclodextrin with 50 mM tricine (pH 8.2) twice per day (with a separation of 7 hours) by oral gavage followed by blood sampling at 0.5, 1, 2, 4, 8, 12 and 24 hours. 0.1 mL of blood was collected twice from each animal over the experiment into Li-Heparin Microvette tubes (Sardtedt AG & Co; Numbrecht, Germany) and centrifuged to prepare to plasma. Tolerability of compound **10** was tested by dosing 5 naïve mice twice per day with 100 or 30 mg/kg for 7 days with observation for 7 subsequent days. For evaluation of *in vivo* efficacy, C57BL/6J mice were infected by the aerosol route as previously described(30). After 14 days, groups of 10 mice were dosed with compound **10** given by oral gavage of either 15 mg/kg or 30 mg/kg twice a day. The higher dose group developed signs of distress after 1 week and so that group was dose deescalated to 30 mg/kg once a day. Control groups were dosed with vehicle control (10% (2-Hydroxypropyl)-β-cyclodextrin) with 50 mM tricine (pH 8.2) or 10 mg/kg Rifampicin. After 2 and 4 weeks of treatment, groups of 5 mice were euthanized and appropriate dilutions in 7H9 medium of lung and spleen homogenates plated on 7H11/OADC plates for CFU enumeration.

Pharmacokinetic analysis of pyrimidinetriones. Pharmacokinetic plasma samples were analyzed by an Agilent 1200 Infinity HPLC with Agilent 6460C Triple quadrupole mass

selective detector (LC-QqQ) utilizing electrospray ionization (ESI). Samples were prepared by mixing 50 µL serum with 50 µL labetalol^{TM} internal standard (IS), 20 µL water or spike solution, followed by 400 µL acetonitrile/methanol 3:1 for protein precipitation. Samples were centrifuged 13 k rpm x 5 min and 5 µL supernatant injected into a 2.1 x 50 mm EclipsePlus C18 1.8 µm column utilizing aq. 0.1% formic acid (solvent A) and acetonitrile w 0.1% formic acid (solvent B). Solvent gradient program was 8% B hold 0.5 minutes to 95% B in 4.5 minutes with flow rate 0.8 ml/min.

MRM transition for compound **10** was detected as $[M-H]^-$ precursor (Q1), CEV 24V, and 155 product ion(Q2) negative mode, and IS detected as $M+H^+$ precursor (Q1), CEV 8V, and 311.2 product ion (Q2) positive mode.PK prameters were calculated using PK macros in Excel.

ACKNOWLEDGEMENTS

This work was funded in part by the Intramural Research Program of NIAID (AI000693-25), by grants from the Foundation for the National Institutes of Health (BARRY11HTB0) with support from the Bill & Melinda Gates Foundation (OPP1024021). The funders had no role in study design, data collection and interpretation, or the decision to submit the work for publication. We gratefully acknowledge the assistance of Danielle Weiner in animal efficacy experiments and Aashish Srivastava for preparing samples for sequencing.

ABBREVATIONS

559 *Mtb, Mycobacterium tuberculosis*; Kan, kanamycin; INH, isoniazid; RIF, rifampicin; MIC,
560 minimum inhibitory concentration; AUC, area under the curve; CFU, colony-forming
561 units; ICP-MS, inductively-coupled plasma mass spectrometry.

562

563 **REFERENCES**

564 1. Leung CC, Lange C, Zhang Y. 2013. Tuberculosis: current state of knowledge: an epilogue.
565 Respirology 18:1047-55.
566 2. Horsburgh CR, Jr., Barry CE, 3rd, Lange C. 2015. Treatment of Tuberculosis. N Engl J Med
567 373:2149-60.
568 3. Barry CE. 2011. Lessons from seven decades of antituberculosis drug discovery. Curr Top Med
569 Chem 11:1216-25.
570 4. Gopal P, Dick T. 2014. Reactive dirty fragments: implications for tuberculosis drug discovery.
571 Curr Opin Microbiol 21:7-12.
572 5. Libardo JMD, Boshoff HI, Barry CE, 3rd. 2018. The present state of the tuberculosis drug
573 development pipeline. Curr Opin Pharmacol 42:81-94.
574 6. Maguire ME. 2006. Magnesium transporters: properties, regulation and structure. Front Biosci
575 11:3149-63.
576 7. Groisman EA, Hollands K, Kriner MA, Lee EJ, Park SY, Pontes MH. 2013. Bacterial Mg2+
577 homeostasis, transport, and virulence. Annu Rev Genet 47:625-46.
578 8. Buchmeier N, Blanc-Potard A, Ehrt S, Piddington D, Riley L, Groisman EA. 2000. A parallel
579 intraphagosomal survival strategy shared by mycobacterium tuberculosis and Salmonella
580 enterica. Mol Microbiol 35:1375-82.
581 9. Goodsmith N, Guo XV, Vandal OH, Vaubourgeix J, Wang R, Botella H, Song S, Bhatt K, Liba A,
582 Salgame P, Schnappinger D, Ehrt S. 2015. Disruption of an M. tuberculosis membrane protein
583 causes a magnesium-dependent cell division defect and failure to persist in mice. PLoS Pathog
584 11:e1004645.
585 10. Walters SB, Dubnau E, Kolesnikova I, Laval F, Daffe M, Smith I. 2006. The Mycobacterium
586 tuberculosis PhoPR two-component system regulates genes essential for virulence and complex
587 lipid biosynthesis. Mol Microbiol 60:312-30.
588 11. Garcia-del Portillo F, Foster JW, Maguire ME, Finlay BB. 1992. Characterization of the micro-
589 environment of Salmonella typhimurium-containing vacuoles within MDCK epithelial cells. Mol
590 Microbiol 6:3289-97.
591 12. Piddington DL, Kashkouli A, Buchmeier NA. 2000. Growth of Mycobacterium tuberculosis in a
592 defined medium is very restricted by acid pH and Mg(2+) levels. Infect Immun 68:4518-22.
593 13. Sassetti CM, Boyd DH, Rubin EJ. 2003. Genes required for mycobacterial growth defined by high
594 density mutagenesis. Mol Microbiol 48:77-84.
595 14. Lamichhane G, Zignol M, Blades NJ, Geiman DE, Dougherty A, Grosset J, Broman KW, Bishai WR.
596 2003. A postgenomic method for predicting essential genes at subsaturation levels of
597 mutagenesis: application to Mycobacterium tuberculosis. Proc Natl Acad Sci U S A 100:7213-8.
598 15. Lee W, VanderVen BC, Fahey RJ, Russell DG. 2013. Intracellular Mycobacterium tuberculosis
599 exploits host-derived fatty acids to limit metabolic stress. J Biol Chem 288:6788-800.

16. Thomas ST, VanderVen BC, Sherman DR, Russell DG, Sampson NS. 2011. Pathway profiling in Mycobacterium tuberculosis: elucidation of cholesterol-derived catabolite and enzymes that catalyze its metabolism. J Biol Chem 286:43668-78.
17. Anderson CM, Norquist BA, Vesce S, Nicholls DG, Soine WH, Duan S, Swanson RA. 2002. Barbiturates induce mitochondrial depolarization and potentiate excitotoxic neuronal death. J Neurosci 22:9203-9.
18. Marroquin LD, Hynes J, Dykens JA, Jamieson JD, Will Y. 2007. Circumventing the Crabtree effect: replacing media glucose with galactose increases susceptibility of HepG2 cells to mitochondrial toxicants. Toxicol Sci 97:539-47.
19. Lopez Quezada L, Silve S, Kelinske M, Liba A, Diaz Gonzalez C, Kotev M, Goullieux L, Sans S, Roubert C, Lagrange S, Bacqué E, Couturier C, Pellet A, Blanc I, Ferron M, Debu F, Li K, Aubé J, Roberts J, Little D, Ling Y, Zhang J, Gold B, Nathan C. 2019. Bactericidal Disruption of Magnesium Metallostasis in Mycobacterium tuberculosis Is Counteracted by Mutations in the Metal Ion Transporter CorA. mBio 10:e01405-19.
20. Kelley LA, Mezulis S, Yates CM, Wass MN, Sternberg MJ. 2015. The Phyre2 web portal for protein modeling, prediction and analysis. Nat Protoc 10:845-58.
21. Mouscadet JF, Tchertanov L. 2009. Raltegravir: molecular basis of its mechanism of action. Eur J Med Res 14 Suppl 3:5-16.
22. Zhang YJ, Reddy MC, Ioerger TR, Rothchild AC, Dartois V, Schuster BM, Trauner A, Wallis D, Galaviz S, Huttenhower C, Sacchettini JC, Behar SM, Rubin EJ. 2013. Tryptophan biosynthesis protects mycobacteria from CD4 T-cell-mediated killing. Cell 155:1296-308.
23. Laarakker MC, van Lith HA, Ohl F. 2011. Behavioral characterization of A/J and C57BL/6J mice using a multidimensional test: Association between blood plasma and brain magnesium-ion concentration with anxiety. Physiology & Behavior 102:205-219.
24. Wang D, Zhang Z, Lu X, Feng Y, Luo K, Gan J, Yingxue L, Wan J, Li X, Zhang F, Tu Z, Cai Q, Ren X, Ding K, Ding K. 2011. Hybrid compounds as new Bcr/Abl inhibitors. Bioorganic & medicinal chemistry letters 21:1965-1968.
25. Duckworth BP, Wilson DJ, Nelson KM, Boshoff HI, Barry CE, 3rd, Aldrich CC. 2012. Development of a selective activity-based probe for adenylating enzymes: profiling MbtA Involved in siderophore biosynthesis from Mycobacterium tuberculosis. ACS Chem Biol 7:1653-8.
26. Oh S, Park Y, Engelhart CA, Wallach JB, Schnappinger D, Arora K, Manikkam M, Gac B, Wang H, Murgolo N, Olsen DB, Goodwin M, Sutphin M, Weiner DM, Via LE, Boshoff HIM, Barry CE, 3rd. 2018. Discovery and Structure-Activity-Relationship Study of N-Alkyl-5-hydroxypyrimidinone Carboxamides as Novel Antitubercular Agents Targeting Decaprenylphosphoryl-beta-d-ribose 2'-Oxidase. J Med Chem 61:9952-9965.
27. Alland D, Steyn AJ, Weisbrod T, Aldrich K, Jacobs WR, Jr. 2000. Characterization of the Mycobacterium tuberculosis iniBAC promoter, a promoter that responds to cell wall biosynthesis inhibition. J Bacteriol 182:1802-11.
28. Ioerger TR, Feng Y, Ganesula K, Chen X, Dobos KM, Fortune S, Jacobs WR, Jr., Mizrahi V, Parish T, Rubin E, Sassetti C, Sacchettini JC. 2010. Variation among genome sequences of H37Rv strains of Mycobacterium tuberculosis from multiple laboratories. J Bacteriol 192:3645-53.
29. Park Y, Pacitto A, Bayliss T, Cleghorn LA, Wang Z, Hartman T, Arora K, Ioerger TR, Sacchettini J, Rizzi M, Donini S, Blundell TL, Ascher DB, Rhee K, Breda A, Zhou N, Dartois V, Jonnala SR, Via LE, Mizrahi V, Epemolu O, Stojanovski L, Simeons F, Osuna-Cabello M, Ellis L, MacKenzie CJ, Smith AR, Davis SH, Murugesan D, Buchanan KI, Turner PA, Huggett M, Zuccotto F, Rebollo-Lopez MJ, Lafuente-Monasterio MJ, Sanz O, Diaz GS, Lelievre J, Ballell L, Selenski C, Axtman M, Ghidelli-Disse S, Pflaumer H, Bosche M, Drewes G, Freiberg GM, Kurnick MD, Srikumaran M, Kempf DJ, Green SR, et al. 2017. Essential but Not Vulnerable: Indazole Sulfonamides Targeting Inosine

Monophosphate Dehydrogenase as Potential Leads against Mycobacterium tuberculosis. ACS Infect Dis 3:18-33.

30. Singh R, Barry CE, 3rd, Boshoff HI. 2010. The three RelE homologs of Mycobacterium tuberculosis have individual, drug-specific effects on bacterial antibiotic tolerance. J Bacteriol 192:1279-91.

655 **TABLE 1** Antitubercular activity of pyrimidinetrione amide analogs

Compound[a]	Chemical Structure R	MIC (μM) 7H9[b]	MIC (μM) GAST[c]
1	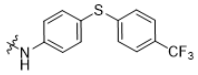	0.2	0.29
2		2.24	1.49
3		>50	9.4
4	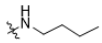	25	12.5
5	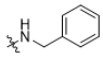	50	0.39
6	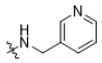	>50	>50
7	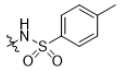	>50	37
8		>50	>50

656 [a] All compound **1–8** are known molecules. MIC of compound against *Mtb* H37Rv in [b] Middlebrook 7H9/BSA
657 containing glucose/glycerol/Tween80, [c] GAS medium with Tween80.

658

659

TABLE 2 Antitubercular activity and cytotoxicity of pyrimidinetrione amide analogs

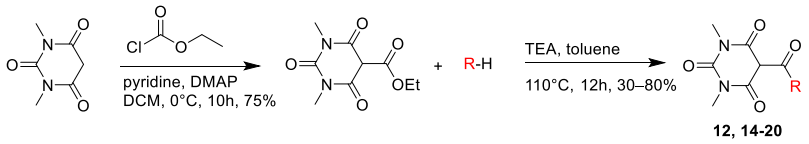

12, 14-20

Compound[a]	Chemical Structure R	MIC (μM) 7H9[b]	GAST[c]	Butyrate[d]	7H9 (*corA*:E212D)[e]	Cytotoxicity (IC_{50}, μM) Glucose[f]	Galactose[g]
1	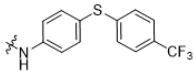	0.20	0.29	0.10	>50	29.5	5.50
2		2.24	1.49	ND	ND	ND	ND
9	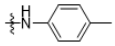	1.20	0.78	1.56	>50	>100	>100
10	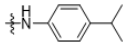	0.59	0.20	3.13	6.25	>100	>100
11	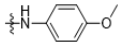	3.10	1.56	3.13	3.10	72.5	23.0
12	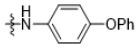	0.78	0.20	0.59	6.25	26.6	3.50
13	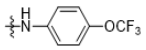	0.20	0.07	1.17	3.13	24.6	3.80
14	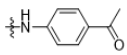	3.10	4.69	3.13	25.0	8.54	2.10
15	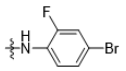	0.78	0.20	1.17	9.38	19.0	5.20
16	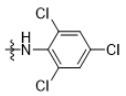	6.30	1.17	6.25	>50	>100	50
17	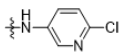	4.70	3.13	3.13	>50	>100	28.0
18		>50	>50	>50	>50	ND	ND
19	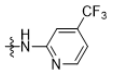	>50	>50	>50	>50	ND	ND
20	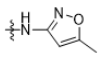	9.38	2.34	50	>50	ND	ND

[a] Compound **1**, **2**, **9–11**, **13** are known molecules. MIC of compounds against *Mtb* H37Rv in [b] Middlebrook 7H9/BSA containing glucose/glycerol/Tween80, [c] GAS medium with Tween80, [d] Middlebrook 7H9/BSA/Tyloxapol/butyrate/0.1 mM nitrite/pH 6.0. [e] MIC of compounds against CorA:E212D mutant Mtb strain in Middlebrook 7H9/BSA containing

665 glucose/glycerol/Tween80. [f] Cytotoxicity of compound tested against HepG2 cells in DMEM/10% FBS supplemented
666 with glucose. [g] Cytotoxicity of compound tested against HepG2 cells in DMEM/10% FBS with galactose.

667

668 **TABLE 3** Mutations identified in pyrimidinetrione amide-resistant *Mtb* strains

Strain	Polymorphisms
E2.1	*corA*:E212D, 4221182:T>C (-30 bp upstream of *Rv3776*)
E2.2	*corA*:A317S, *Rv0275c*:S233S, 3281706 -G (in aa 342/2111 of *mas*)
E2.6	Same as E2.2

669

670 **TABLE 4** Thermostability of CorA in the presence of metal cations, EDTA and compound **10**.

CorA + additive	Melting temperature (℃)
none	55
0.125 mM $MgCl_2$	70
1 mM compound **10**	≥95
1 mM compound **10** / 0.125 mM $MgCl_2$	≥95
1 mM EDTA / 0.125 mM $MgCl_2$	≥95

671

672 **TABLE 5** The apparent dissociation constant (K_d(app)) of CorA with metal cations and
673 compound **10**.

CorA additives in fluorescence shift assay	K_d(app) μM
Mg^{2+}	47.5 ± 3.0
Co^{2+}	205 ± 18
Compound **10**	20.0 ± 4.3
Compound **10** / 1 mM Mg^{2+}	24.1 ± 6.3
Compound **10** / 1 mM Co^{2+}	21.8 ± 4.1

674

675

676 **FIGURE LEGENDS**

677 **FIG 1** The pyrimidinetrione amide scaffold inhibits Mg^{2+} uptake by Mtb. (A) Magnesium
678 dependence of the pyrimidinetrione amide MIC against *Mtb* performed in Mg^{2+}-free
679 media with the indicated concentrations of Mg^{2+}. (B) Co^{2+} dependence of the
680 pyrimidinetrione amide MIC against *Mtb* performed in Co^{2+}-free media with the indicated
681 concentrations of Co^{2+}. (C) Fold change in intracellular Mg^{2+} concentration as measured
682 by ICP-MS compared to vehicle (DMSO) control after 24h of treatment with moxifloxacin
683 (Mox) or compound **10** at 1- or 10-fold MIC concentration in 7H9 medium which
684 contains 0.4 mM Mg^{2+}. Significance between groups was determined by Tukey's
685 Multiple Comparison Test with significance set at P values less than 0.05.

686 **FIG 2** Magnesium and the pyrimidinetrione scaffold bind to the CorA transporter
687 protein. The thermostability of recombinantly expressed CorA from *Mtb* was measured
688 with (A) no ligand, (B) 0.125 mM $MgCl_2$ and (C) 0.125 mM $MgCl_2$ with or without 1.0 mM
689 compound **10**. Protein was pre-incubated at room temperature with the indicated
690 ligands before heating to the indicated temperatures in a thermocycler. Protein
691 precipitates were removed by filtration and soluble protein analyzed by SDS-PAGE.

692 **FIG 3** The pyrimidinetrione amide scaffold is cidal against replicating as well as non-
693 replicating *Mtb* i*n vitro* and *ex vivo*. (A) Kill kinetics of compound **10** against *Mtb* during
694 active replication *in vitro* as compared to negative (DMSO) and positive (5 µg/mL RIF)
695 controls. (B) Anaerobic cidal activity of compounds **9**, **10** and **20** as compared to
696 negative (untreated, DMSO and 1 µg/mL INH) and positive (100 µM metronidazole)
697 controls after 7 days of compound exposure. (C) Efficacy of compounds **1, 9**, **10** and **16**

during growth of *Mtb* in J774 macrophages as compared to the negative (DMSO) and positive (0.5 and 5 µg/mL RIF) controls. Black horizontal bar indicates inoculum (day 0).

FIG 4 The pyrimidinetrione amide lacks in vivo efficacy. (A) PK profile of compound **10** after twice daily administration at 30 mg/kg. (B) *Mtb* bacterial burdens in infected mice after 2 and 4 weeks of once daily or twice daily treatment at 30 and 15 mg/kg, respectively. Treatment was initiated at 2 weeks after aerosol infection of the mice.